ELSEVIER

Contents lists available at ScienceDirect

Chemical Engineering Journal

journal homepage: www.elsevier.com/locate/cej





Analysis of coupled heat & mass transfer during gas hydrate formation in bubble column reactors

Aritra Kar, Vaibhav Bahadur

Walker Department of Mechanical Engineering, The University of Texas at Austin, USA

ARTICLE INFO

Keywords: CO₂ hydrate Bubble column reactor Heat transfer Mass transfer Subcooling gas separation

ABSTRACT

Gas hydrates have promising applications in gas separation, carbon capture, desalination and gas storage. Although there exist several studies on modeling hydrate growth, analysis of the coupled role of heat and mass transfer on hydrate formation has been largely neglected. Presently, we develop a fundamentals-based simulations framework which accounts for mass transfer, heat transfer and various interfacial phenomena associated with gas hydrate formation in a bubble column reactor. We model CO2 separation from syngas via CO2 hydrate formation and validate against experiments from another study. This model is used to quantify the impact of various operating parameters (gas flow rate, bubble size, reactor pressure, inlet gas temperature, reactor geometry) on hydrate formation rate and gas-to-hydrate conversion factor. Results provide several insights related to the intricate transport phenomena that underlie hydrate formation. Firstly, we highlight the adverse impact of inadequate heat dissipation on hydrate formation rate and conversion factor. This is particularly important for high gas flow rates, wherein high hydrate formation rate triggers substantial temperature rise. Enhancing thermal conductivity of hydrate forming media can significantly enhance formation, with the conversion factor seen to double. Secondly, simulations show that bubbles < 100 μm diameter are essential to realize high growth rates. Thirdly, increasing reactor pressure can significantly improve the maximum theoretical separation efficiency for CO2 to > 90 %. Fourthly, precooling the inlet gas enhances hydrate formation rates by upto 5 %. Overall, this work outlines a novel approach to modeling hydrate formation and provides a tool for process optimization.

1. Introduction

Gas hydrates are crystalline, ice-like solids that form from gas and water at low temperatures and high pressures [1,2]. Gas hydrates have several applications in fields like carbon capture and sequestration, desalination, gas separation, storage and transportation [3]. Such applications require rapid hydrate formation, therefore significant research has focused on enhancing the kinetics of hydrate formation through efficient use of chemical promoters and innovative design of reactors and processes. Although there exist several experimental studies on hydrate formation, there is a relative lack of comprehensive simulations that analyze hydrate growth in reactors. Most existing models treat heat and mass transfer separately, and there is a lack of understanding on the coupling between the phase-change kinetics associated with hydrate formation, and heat transfer limitations in the system [4]. Inadequate understanding of the heat and mass intricacies associated with hydrate formation influence the ability to accurately

model hydrate formation in pipelines, hydrate dissociation in porous media and hydrate formation in nature. This study seeks to overcome current limitations in the understanding of coupled heat and mass transfer and develop a simulation framework to study gas separation via hydrate formation in a bubble column reactor.

Modeling of hydrate growth kinetics in reactors is several decades old with the first efforts starting in the 1980s [5]. Early efforts modeled hydrate growth using theories of interphase mass transfer at the gas-liquid interfaces coupled with population balance of hydrate particles [6–8]. Such theories work quite well during initial stages of hydrate formation; however, as more hydrates are deposited at the gas-liquid interface, the hydrate layer presents strong diffusion resistance to gas and water which must be accounted for. Recently, the influence of mass transfer resistances associated with the hydrate layer has been incorporated using the shrinking core models, phase-field simulations and other formulations [9–12]. Most of these models have implemented a traditional stirred batch reactor for hydrate formation; however, recent experimental studies have shown that other types of

E-mail address: vb@austin.utexas.edu (V. Bahadur).

^{*} Corresponding author.

Nomenclature		Q	Gas flow rate per unit area (L/m ² min)
		T_{pc}	Gas flow inlet temperature (K)
ρ_{g}	Density of gas (kg/m ³)	P_{eq}	Equilibrium pressure (MPa)
η	Bubble radius (μm)	k	Thermal conductivity (W/mK)
C_D	Drag coefficient	R	Radius of the reactor (m)
A_b	Surface area of bubble (μm²)	A_{cs}	Reactor cross sectional area (m ²)
R	Universal Gas Constant (J/mol K)	T	Temperature (K)
M_h	Molar mass of hydrate (kg)	z	Axial coordinate (m)
m	Hydrate mass on the bubble (kg)	$ u_{ m terminal}$	Terminal bubble velocity (m/s)
ν	Velocity of bubble (m/s)	η_s	Bubble radius after sparging (µm)
ρ_w	Density of water (kg/m³)	A_f	Hydrate film area (μm²)
g	Acceleration due to gravity (m/s ²)	ť	Film thickness (μm)
x	Mole fraction of hydrate former	c_{eq}	Equilibrium gas concentration (mol/m³)
g_f	Growth factor	h_{top}	heat transfer coefficient above the water column (J/m ² K)
$\stackrel{\circ}{P}$	Total pressure inside bubble (MPa)	H	Height of water column (m)
γ	Gas water surface tension (N/m)	N	Number density of bubbles (m ⁻³)
Z	Compressibility factor	r	Radial coordinate (m)
k_m	Mass transfer coefficient (m/s)	N_2	Moles of non-participating gas inside gas bubble (mol)
x_1	Initial mole fraction	ΔH	Heat of hydrate formation (kJ/mol)
c	Gas concentration $(\text{mol/m}^3)Z_{eq} = Z(P_{eq}, T)$	n	Moles of gas (mol)
$T_{ m inf}$	Temperature of coolant (K)		-

reactors can result in faster hydrate formation [13–17]. Specifically, bubble column reactors lead to high rates of gas hydrate formation due to large gas—liquid interfacial area [18]. Such a reactor is generally operated in the sparse bubbly regime with low superficial gas velocities to prevent large-scale coalescence of bubbles or slug flow. Also, smaller gas bubbles allow higher residence times of the bubble inside water due to low rise velocities; this improves the conversion efficiency of gas into hydrates. In this study, we develop a simulation framework for the continuous operation of bubble column reactor forming hydrates from bubbles of gas mixtures.

The earliest studies utilizing bubble column reactors for both methane and carbon dioxide hydrate growth are more than a decade old [19,20]. Several experimental studies have targeted gas separation from coal-bed gas and syngas, for separating methane and carbon dioxide, respectively [18,21–23]. Experimental studies have been conducted on mixed clathrate hydrates of cyclopentane-methane and natural gas [24,25]. All such studies sparge the gas via bubbles and report high hydrate formation rates with minimal use of thermodynamic promoters. Bubble column reactors have also been used in hydrate-based desalination applications [26]. All of these highlight the potential uses of bubble column reactors for rapid hydrate formation for a variety of applications.

The present study develops a modeling framework to understand and optimize the operation of bubble column reactors for gas hydrate formation. There exists a study on modeling hydrate growth in bubble column reactor operating in the slug flow regime [27], however the influence of heat transfer on hydrate growth kinetics were not considered. Moreover, modern experimental methods operate the bubble column reactor in a sparse bubbly regime rather than slug flow regime, to increase gas—water contact area. Hydrate growth in bubbly flows is also encountered during hydrate formation in pipelines and oil & gas wells and is an active area of research [28]. The physics of hydrate growth in pipelines is different from hydrate growth in reactors due to large-scale agglomeration, breakage of bubbles and multiphase flow encountered in the former. In this study, we simulate sparse bubbly flow of syngas with small bubbles (of size $<200~\mu m$) in a bubble column reactor.

Hydrate crystallization on bubbles can be approximated using a film growth model on the bubble–liquid interface; such ideas have been used for modeling hydrate growth in subsea natural gas pipelines [29,30]. The present group has previously shown that hydrate film growth can be

effectively modeled using molecular diffusion of gas near the gas-water interface [31]. In this study, we utilize this model to quantify the phasechange rate of hydrate, on a bubble rising inside the reactor. As discussed before, bubble column reactors provide high rates of hydrate formation, hence the process can be significantly heat transfer-limited if not designed appropriately. Hydrate formation is akin to a crystallization process and is accompanied by a high exothermic heat of formation [32]. This heat, if not dissipated from the reactor, will increase the temperature inside the reactor and reduce the driving force for hydrate formation. A previous study from this group explained this concept in terms of the actual subcooling available for hydrate formation versus the apparent subcooling [33]. Apparent subcooling is the difference between the equilibrium temperature of hydrate formation and the experimentally set temperature ($\Delta T_{apprent} = T_{eq} - T_{inf}$), whereas actual subcooling is the difference between the equilibrium temperature and the actual temperature in the reactor ($\Delta T_{actual} = T_{eq} - T$). Due to heat released during hydrate formation, the temperature of the reactor

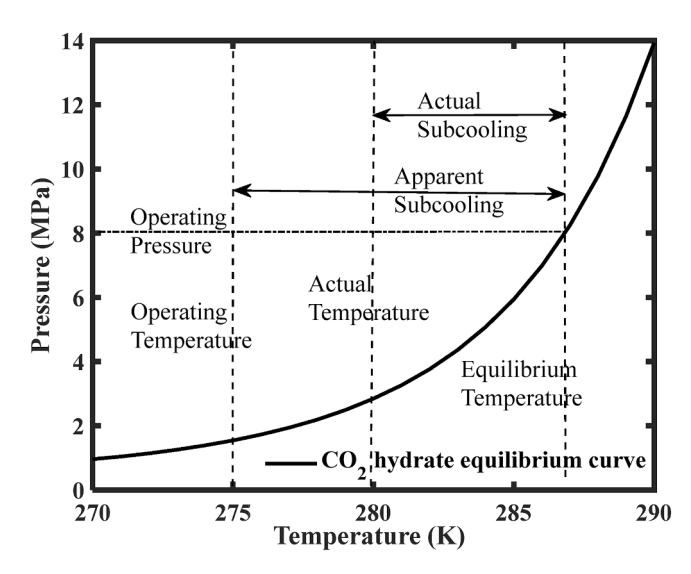


Fig. 1. Difference between apparent subcooling and actual subcooling using CO_2 hydrate equilibrium curve. Equilibrium curve data was adopted from Sloan & Koh [1].

increases and $\Delta T_{actual} < \Delta T_{apparent}$, as seen in Fig. 1. This reduces the driving force for hydrate formation and thereby reduces the mass of hydrate formed. Previous modeling studies do not couple the temperature and intrinsic phase-change kinetics of hydrates [34–37]. For example, Zerpa et al.. considered the rate of hydrate crystallization as the smaller of the mass transport-based prediction and heat transport-based prediction; this formulation assumes that hydrate formation is limited either by mass transfer or by heat transfer [29]. Such a formulation fails to account for cases where hydrate crystallization is not completely mass transfer-limited or heat transfer-limited but rather falls somewhere in between.

The importance of heat removal from a reactor is further evident from several experimental studies, which report a sharp rise in temperature during hydrate formation. Clathrate hydrates with miscible hydrate formers exhibit faster hydrate crystallization and therefore the temperature rises rapidly, resulting in a spike [38,39]. For gas hydrates formed from carbon dioxide or methane, the temperature rises at a slower rate [40,41], however it will reduce the rate of subsequent hydrate formation after some time. Moreover, in reactors where rapid hydrate formation is possible, the influence of reduced driving force due to temperature rise can be significant, resulting in reduced hydrate formation rates. Recently, Chen et al. experimentally showed that improving heat transfer in bubble column reactors can significantly improve the rate of hydrate formation [18]. The present work can be used to develop tools to quantify the impact of enhanced heat dissipation (via higher thermal conductivity), and other parameters on hydrate formation.

2. Mathematical model and solution methods

The mathematical model developed in this study simulates the continuous operation of a bubble column reactor, which separates a target gas from a binary mixture of gases via formation of gas hydrate. In this study, separation of $\rm CO_2$ gas from syngas (mixture of 40 % $\rm CO_2$ and 60 % $\rm H_2$) via formation of $\rm CO_2$ hydrates is studied. It is noted that $\rm H_2$ hydrates will not be formed, since they require much higher pressures to form, as compared to $\rm CO_2$ hydrates. Fig. 2a shows the schematic of such a setup, where the reactor is maintained at a constant pressure and bubbles of the gas mixture are sparged from the bottom. Hydrates accumulate on the bubbles as they rise inside the water column of the reactor. Subsequently, these hydrates are deposited either on the gas—water interface or drop down to the bottom of the reactor from where

they are removed as hydrate slurries (shown in Fig. 2a). Water consumed or removed as slurry from the reactor is continuously replenished for steady-state operation. As mentioned earlier, the reactor is operated in the sparse bubbly regime and a steady-state mathematical model is developed assuming a continuum field of bubbles in the water medium. Hence, the parameters of the bubbles, like velocity, radius etc. are described using a Eulerian description inside the computation domain (Fig. 2b). More details on the formulation, solution methods and assumptions are provided subsequently. Codes are developed in Python and are included in the supplementary information. Details of the code are documented (in supplementary information) and in-line commenting enable the readability/usability of the codes.

2.1. Governing equations

The governing equations for this system consists of 6 equations in 6 variable fields, v,η,m,x,N,T . A description of all variables is provided in the nomenclature. Equation (1) governs the velocity field of the bubble and is a force balance equation. The equation describes the acceleration of the bubbles due to buoyancy of the gas inside the bubbles. Bubble motion is opposed by the drag force due to the surrounding fluid and the hydrate mass on the bubbles. It should be noted that for the case of laminar flow over a sphere (commonly referred to as Stokes drag), drag force is proportional to ν . However, the drag force in this analysis was assumed to be proportional to v^2 (similar to that encountered in turbulent flow) for multiple reasons. Firstly, hydrates accumulating on a bubble rising inside the reactor do not preserve the spherical shape of the bubble [21]. Secondly, the surface texture of hydrates is not very smooth [42,43], which can trip the flow over such surfaces to turbulent even at low Reynolds numbers. Finally, many engineered flows are turbulent (to enhance mass and heat transfer). For all these reasons we believe that a turbulent drag approximation is more appropriate for the present problem. The boundary condition at the bottom of the reactor is the terminal velocity of the bubble without any hydrate mass.

$$\left(m + \frac{4}{3}\pi\rho_g \eta^3\right) v \frac{\partial v}{\partial z} = \left(\rho_w - \rho_g\right) \frac{4}{3}\pi\eta^3 g - mg - \frac{1}{2}\rho_w C_D A_b v^2$$

$$BC: \ v(0) = v_{\text{terminal}}$$
(1)

Equation (2) tracks the evolution of bubble radius in the reactor. This equation is derived based on gas laws while accounting for the gas consumption due to hydrate crystallization and other factors like surface

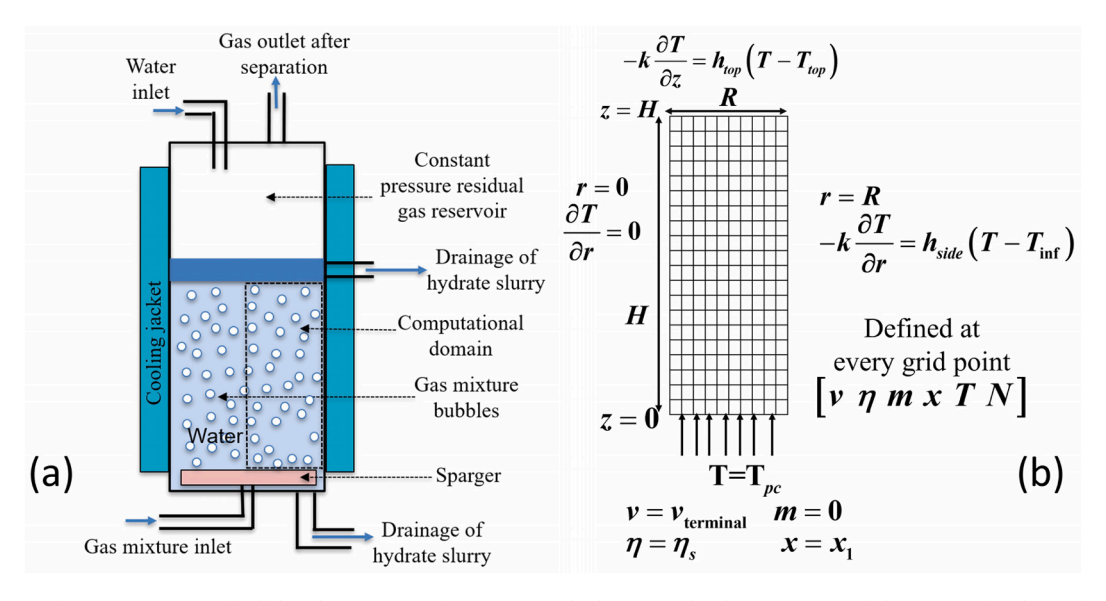


Fig. 2. (a) Schematic showing operation of bubble column reactors for continuous hydrate growth. The computational domain used in this study is marked with a dotted boundary (b) Details associated with the computational domain.

tension, hydrostatic pressure, temperature gradients etc. The compressibility factor Z is calculated using the Peng-Robinson equation of state [44]. The Peng-Robinson equation of state is implemented through the compressibility factor Z in equation (2) (Table 1 in ref [44]). The compressibility factor is solved as a cubic equation and the root of the equation that falls within 0 and 1 is considered. The last term dZ/dz is neglected in this study since strong gradients of compressibility factor are not expected.

$$\left(3P - \frac{2\gamma}{\eta}\right)\frac{\partial\eta}{\partial z} = -\frac{3ZRT}{4\pi\eta^2 M_h}\frac{\partial m}{\partial z} + \rho_w g\eta + \frac{P\eta}{T}\frac{\partial T}{\partial z} + \frac{P}{Z}\frac{dZ}{dz}
BC: \eta(0) = \eta_s$$
(2)

Equation (3) describes the evolution of hydrate mass and the mole fraction of the hydrate-forming gas inside the bubble. The increase in hydrate mass on the bubble is due to hydrate crystallization which consumes gas inside the bubble and decreases its mole fraction. As mentioned earlier, hydrate crystallization is modeled as film growth on the bubble. The concentration of the hydrate forming gas is multiplied by the mole fraction \boldsymbol{x} to account for the partial pressure of the gas and not the total pressure of the gas mixture. The boundary condition at the bottom of the reactor is zero-hydrate mass on the bubbles and the initial mole fraction of the incoming gas mixture.

details on these assumptions are outlined later. Equation (6) predicts the total pressure inside the bubble at any point inside the reactor.

$$Nv = \frac{3Q}{4\pi n^3 A_{cr}} \tag{5}$$

$$P(z) = P_{op} + \rho_w g(H - z) + \frac{2\gamma}{\eta(z)}$$
(6)

A detailed derivation of all equations in this section is available in the supplementary information. The set of Eqs. (1)–(6) describe the physics of hydrate growth inside a bubble column reactor operating in the sparse bubbly flow regime. Fluid dynamic equations in the water phase has not been included in the present model to reduce the complexity of the model and enhance convergence. The movement of bubbles in bubble column reactors and airlift reactors are known to setup convective flow patterns in the vertical direction of the reactor. This is discussed in more detail in the next section and is beyond the scope of this work.

2.2. Assumptions in the model

There are several assumptions underlying this model, which are listed ahead. Most of them are justified due to the operational conditions of the reactor; moreover, they simplify the mathematical model to a

$$v\frac{\partial m}{\partial z} = k_m M_h A_f \left(xc - c_{eq}\right), x = \frac{x_1 - \frac{m}{N_2 M_h} (1 - x_1)}{1 - \frac{m}{N_2 M_h} (1 - x_1)}, A_f = 2\pi \eta g_f t, \ c = \frac{P}{ZRT}, \ c_{eq} = \frac{P_{eq}}{Z_{eq}RT}$$

$$BC: \ m(0) = 0, \ x(0) = x_1$$
(3)

The temperature field in the reactor is governed by the steady-state energy equation (Eq. (4)) with heat generation due to hydrate crystallization. This equation takes the form of a 2D Poisson equation in cylindrical coordinates. This equation governs the propagation of heat waves in the reactor generated on the population of bubbles upon the recalescence of hydrates. The thermal conductivity is assumed to be that of water. Four temperature boundary conditions are implemented on the top and bottom of the reactor, external cylindrical surface of the reactor and the centerline of the reactor. A natural convection boundary condition is implemented on the top of the reactor. Forced liquid coolingbased convection is imposed on the external cylindrical surface of the reactor. Heat transfer coefficients are assumed to be 10 W/m²K and 5000 W/m²K on the top and sides of the reactor, respectively. The liquid coolant is considered to be at 0 °C. Due to symmetry, a zero Neumann boundary condition is used on the centerline of the reactor. A Dirichlet boundary condition is used at the bottom of the reactor corresponding to the temperature of the pre-cooled gas.

$$k\left(\frac{\partial^{2}T}{\partial r^{2}} + \frac{1}{r}\frac{\partial T}{\partial r} + \frac{\partial^{2}T}{\partial z^{2}}\right) + \frac{Nv\Delta H}{M_{h}}\frac{\partial m}{\partial z} = 0$$

$$BCs: T(0,r) = T_{pc}, -k\frac{\partial T}{\partial z}(H,r) = h_{top}\left(T(H,r) - T_{top}\right)$$

$$-k\frac{\partial T}{\partial r}(z,0) = 0, -k\frac{\partial T}{\partial r}(z,R) = h_{side}\left(T(z,R) - T_{inf}\right)$$
(4)

Equation (5) conserves the number density of bubbles across the reactor. Since our model does not consider bubble coalescence or bubble breakage, the number density of bubbles can be described using a continuity equation without any source/sink term. Also, since lateral forces due to hydrodynamic flow are not considered, bubble density is conserved in the axial direction which simplifies the equation. More

significant extent. Key assumptions include:

- Induction time is short, and nucleation occurs right after the bubble pinches off the sparging plate. We note that this assumption can be justified since hydrate accumulation in and around sparging plate can trigger secondary nucleation of hydrates on the bubbles, which results in very low induction times
- Bubble coalescence is not considered in this model. Superficial velocities are ≪ 1 cm/s, which ensure a sparse bubbly regime [45]. Hence, bubble coalescence will not be a dominating factor. It is noted that bubble coalescence reduces the surface area of the bubbles and increases bubble velocity, which is detrimental to high hydrate growth rates. It is also noted that merging of microbubbles near the sparging plate is a common issue, often limiting the minimum bubble size that can be achieved [46]. Such effects are not considered in this model.
- Hydrodynamic flow of water around the bubbles is not accounted for in this model. Small bubble sizes (<200 µm) results in low Reynolds number flow around the bubble and hence they do not experience significant lateral forces. Therefore, the velocity vectors of the bubbles are aligned in the axial direction. It is noted that the rise of the bubbles will result in flow circulation in the vertical direction of the reactor [47,48]. This would result in an equilibration of heat and mass transfer in the vertical direction. However, such fluid circulation within the reactor would not enhance heat transport in the radial direction which is primarily responsible for transfer of heat to the coolant. We have not included related physics and hydrodynamics in the present model, to reduce complexity. Nevertheless, the incorporation of fluid flow can improve the model further and can be considered for future work. Another option to include hydrodynamics is to combine this study with

computational fluid dynamics-based analysis. However, such an exercise would be challenging since there is very little understanding of two-phase interactions occurring at the hydrate formation interface.

- The hydrodynamic drag is estimated as turbulent drag due to the shape of hydrate-bubble entity and the rough nature of hydrate surface. Our calculations indicate that laminar drag considerations will yield lower rise velocity, higher residence time, and higher rate of hydrate formation. In that sense, this assumption makes our analysis more conservative.
- The phase-change rate on the bubble is not affected by gas or water diffusion limitations through the hydrate layer on the bubble. Diffusion limitations would be significant for thick hydrate layers; with small bubble sizes we expect a thin hydrate layer on the bubble (low mass transfer resistances). Also, due to small bubble sizes, equilibration of heat and mass transfer inside the bubble is of the order of milliseconds which justifies a lumped value of pressure and temperature inside the bubble [49]. This is also evident from estimating the time scales of diffusion and heat transfer within the bubble as R^2/D and R^2/α respectively. Using a scale of radius as $100~\mu m$ and conservative estimates of D and α as 10^{-6} m²/s and 10^{-5} m²/s respectively, we obtain equilibration time scales of 10 ms and 1 ms.

2.3. Procedure for solving the system of equations

The above set of equations are solved on a fine and uniform finite difference grid. The derivatives in equations (1)–(3) are discretized using a 2nd order upwind scheme and (4) is discretized using 2nd order central difference scheme. The boundary conditions are implemented through the discretized equations on the edge cells. Equation (1) is seemingly non-linear; however, it is converted into a linear form in terms of v^2 by rewriting the $v \frac{\partial v}{\partial z}$ term as $\frac{1}{2} \frac{\partial}{\partial z} v^2$. Thereby, it is solved as a linear equation using the matrix inversion method. Equation (2) is solved as a non-linear equation using Newton's iterative method on the finite difference grid. Generally, the convergence is quite fast and happens within 2–3 Newton iterations.

Equation (3) is a non-linear equation and is solved together with the mole fraction of gas inside the bubbles. Newton's iterative method is again used to solve this equation; however, the mole fraction of the gas is also updated continuously after every Newton iteration. Convergence is much slower for this equation than equation (2) and it takes 6–7 iterations to converge. The hydrate mass equation and the mole fraction equation are simultaneously and continuously updated through Newton's iterations until convergence or maximum number of iterations is reached. Equation (4) represents a linear 2D Poisson's equation and it is solved using a matrix inversion method. The columns of the 2D temperature matrix are lined up on a single vector to use a direct matrix inversion. The obtained solution is then rearranged back into a 2D temperature matrix.

The previous two paragraphs discuss the convergence of the individual equations from (1) to (4). Once convergence is achieved for the individual equations, the total residual is calculated by substituting the solutions back into the equations and calculating an RMS value of the residuals of the individual equations. The whole system of equations from (1) to (4) is then iterated continuously until the total residuals reduce to 1E-03. Under-relaxation of equation (3) is necessary during iterations to achieve complete convergence of the set of the equations together. Relaxation factors as low as 0.01 have been used for equation (3) to achieve convergence in some cases. In such cases, the solution converged very slowly and took many hours. Hence, simulations were run using supercomputing resources at Texas Advanced Computing Center (TACC). More details on solution methods are available in the supplementary information.

2.4. Output parameters from simulations

In addition to the process-related variables already described, two other useful parameters are defined: i) steady state hydrate formation rate in the reactor, and ii) conversion factor of incoming gas. The rate of hydrate formation at any height (axial distance) in the reactor is denoted as R(z). Accumulated hydrate mass increases which increasing axial distance, dR/dz > 0. Therefore, the steady-state hydrate formation rate in the reactor is estimated by R(H) where z = H is the maximum height of the water column. The conversion factor, CF is defined as ratio of total moles of gas consumed in hydrate formation inside the reactor to moles of the incoming gas. Similar to the function R(z), conversion factor increases with axial distance and is maximum at z = H. Equations to estimate the R(z) and CF are as follows:

$$R(z) = \int_0^R N(z, r)v(z, r)m(z, r)2\pi r dr$$
 (7)

Conversion factor = CF =
$$\frac{R(z)/M_h}{QA_{cv}x(0)P(0)/RT(0)}$$
 (8)

3. Results

3.1. Operational conditions of the hydrate-forming reactor in the present simulations

In this study, simulations were conducted for an application involving carbon dioxide (CO₂) separation from syngas (consisting of 40 % CO₂ and 60 % H₂). Simulations were conducted to mimic operating parameters in the experiments conducted by Xu et al. [21]. Ref. 21 could then be used to benchmark the present model. Accordingly, total gas flow rates of 27 and 81 L/m²min were simulated. The bubble size was fixed at 50 μ m. Xu et al. [21] conducted these gas separation experiments in a 4 m tall cuboid reactor with a cross-section of 10 cm \times 10 cm[21]. To reconcile our modeling approach (which is based on a cylindrical reactor) with the experiments in Ref. 21, we used a hydraulic diameter of 11.28 cm in the simulations, which ensured the same crosssectional area. Since the experiments were conducted with 0.29 mol% TBAB, the equilibrium conditions for CO₂ hydrate formation become significantly milder. We incorporated a CO2 hydrate equilibrium correlation from Maekawa [50] multiplied by a factor of 1/3rd to account for the addition of TBAB. The resulting correlation with 1/3rd the formation pressures than that of pure CO2 hydrate matched reasonably well with experiments from Mohammadi et al. [51], which used TBAB as a promoter.

The film thickness for CO₂ hydrate was assumed to be 0.1 μ m[52,53] and growth factor, g_f was assumed to be a constant value of 0.25. The growth factor varies between 0 and 0.5; a value of 0.5 corresponds to the maximum rate of growth of the film. The growth factor represents an average circumferential length on a bubble over which film growth occurs. This factor is maximum if the film growth is occurring on a diametrical circumference. The factor essentially accounts for a two-dimensional growth on the surface whereas the film growth model is one-dimensional. It should be noted that this parameter will vary across reactors due the nature of film growth on the bubble surface. The mass transfer coefficient due to diffusion of CO₂ during the hydrate crystallization process is assumed to be 0.01 m/s, based on our previous work on film growth of hydrates [31]. Specific values of each of the parameters used in this simulation are available in the properties.py file attached as codes in the supplementary information.

3.2. Results of simulations of the baseline conditions of the hydrate forming reactor

This section details the results of the simulations for the abovementioned operating conditions of the reactor (referred to as baseline

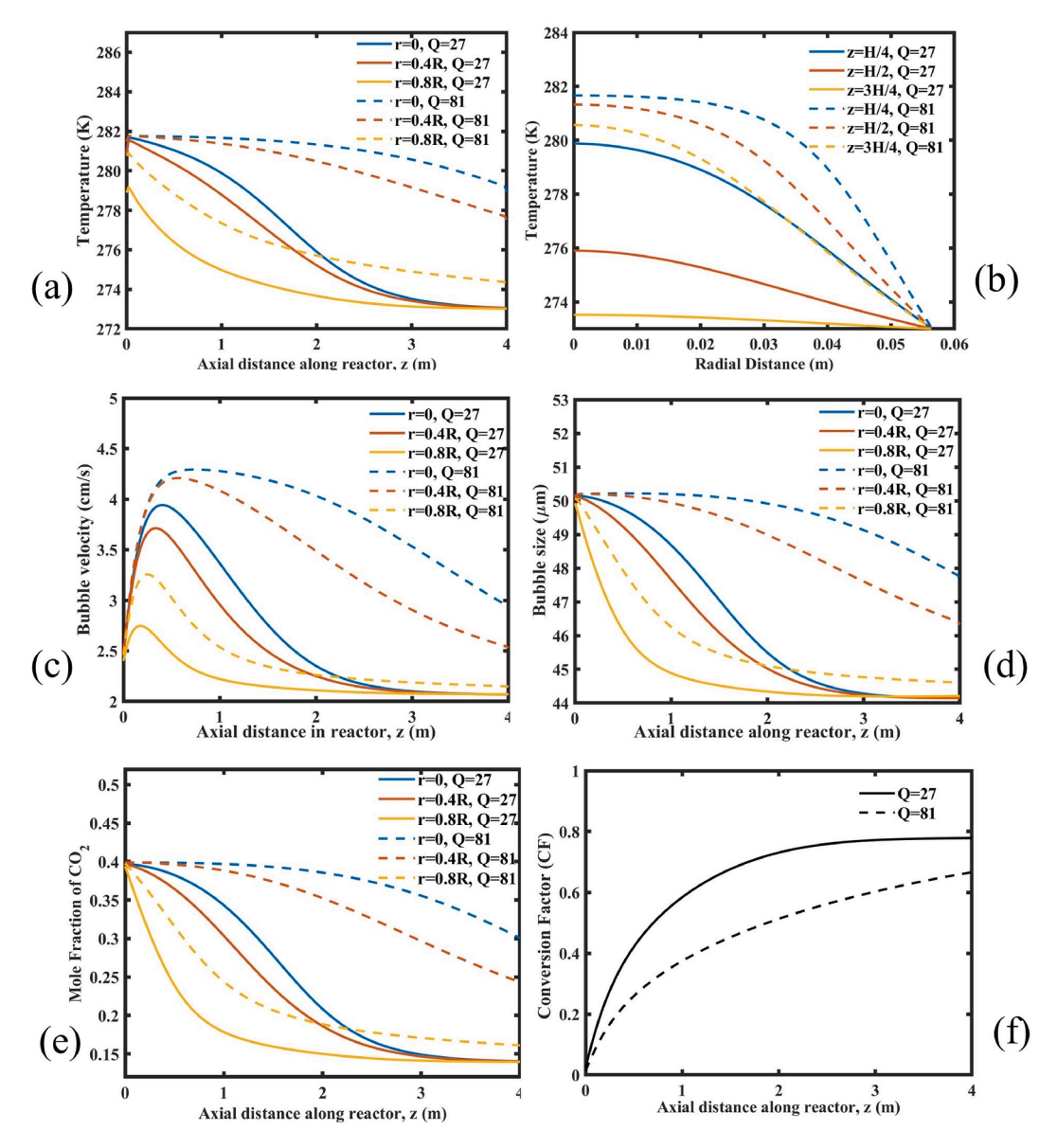


Fig. 3. (a) Axial temperature variation, (b) radial temperature variation, (c) axial variation of bubble velocity, (d) axial variation of bubble radius, (e) axial variation of CO_2 mole fraction, and (f) axial variation of conversion factor of CO_2 in the reactor (showing much slower conversion for the higher flow rate). Radius of the reactor is 5.74 cm, height is 4 m and Q is in units of L/m^2 min.

conditions). Fig. 3a, 3b shows the axial and radial variations of temperature in the reactor. Temperatures do not remain constant throughout the reactor but vary significantly both axially and radially. Due to heat released during hydrate formation, the steady-state temperatures are higher than the coolant temperature (273 K in the simulations). Fig. 3a, 3b show the temperature distributions at three different radial distances for flow rates of 27 and 81 L/m²min. The temperature rise in the reactor is greater for the higher flow rate case, since high flow rates translate to high hydrate formation rates and therefore higher heat generation. Temperature rise is mostly observed in the bottom half of the reactor for lower flow rates with a maximum temperature at the centerline of the reactor. As previously discussed, higher temperatures reduce the driving force for hydrate formation and the rate of conversion. For example, in Fig. 3b, at r = 0 and z = H/4, the steady state temperature is 280 K and 281.7 K for Q = 27 and 81 L/m²min, respectively.

The equilibrium temperature for hydrate formation is 281.8 K for these operating conditions. Hence, the actual subcooling available for hydrate formation is about 1.8 K and 0.1 K for the Q=27 and 81 L/

 m^2 min cases, respectively, for r = 0 and z = H/4. The apparent subcooling is set by the coolant temperature, and is 8.8 K. It is clear from these numbers that hydrate growth will be very significantly limited by heat transfer for the high flow rate case, since the actual temperatures are very close to the equilibrium temperature of hydrate formation (Fig. 3a,3b). For the lower flow rate case, hydrate growth will be significantly heat transfer limited in the bottom half of the reactor. We note that such heat dissipation-based limitations also govern crystallization of ice and are modelled using Stephan's problem [54,55]. Stephan's problem is formulated under the assumption that the temperature in the vicinity of a flat ice-water interface is equal to the equilibrium temperature of ice formation $(T = T_{eq})$ which signifies a heat transfer-limited growth. Our simulations yield similar results in some cases of hydrate growth with $T \approx T_{eq}$. Overall, inadequate heat dissipation can significantly reduce the rate of hydrate formation, this is an important outcome of the present study.

Fig. 3c and d shows the axial variation of bubble velocity and the bubble radius in the reactor at three different radial distances for the two flow rates considered in this study. The boundary condition for bubble

velocity at the bottom of the reactor is the terminal velocity of the bubbles with zero hydrate mass on bubbles. Interestingly, our simulations show that the bubble velocity increases in parts of the reactor with higher temperatures; this can be deduced by comparing Fig. 3a and 3c. This can be attributed to the increased buoyancy of the bubbles at higher temperatures which accelerates the bubbles. This phenomenon is detrimental to conversion efficiency of the gas to hydrates as it decreases the residence time of the bubbles in the reactor. For regions in the reactor, where the temperature in the reactor is close to coolant temperatures, the bubble velocity decreases in the axial direction due to larger hydrate masses accumulating on the bubbles which slows down the bubbles. This trend can be observed near the top of the reactor for the case of $Q=27\ L/m^2 min$ and is beneficial to hydrate formation.

Fig. 3d shows a decreasing bubble radius in the axial direction of the reactor due to gas consumption during hydrate formation. As expected, the bubble radius decreases rapidly for the lower flowrate case due to faster hydrate crystallization at lower temperatures in the reactor. Since our syngas mixture consists of 60 % $\rm H_2$, most of the bubble volume is occupied with the lighter gas, which is considered non-participating in hydrate formation.

Fig. 3e shows the axial variation in mole fraction of CO₂ in the bubbles. Near the bottom of the reactor, the mole fraction is 0.4 corresponding to 40 % of CO2 in the syngas. As the bubbles move up the reactor, CO2 is consumed (hydrate formation) which reduces the mole fraction. The mole fraction represents a very similar trend as that of bubble radius. For higher flow rate, hydrate crystallization rate on individual bubbles is slower due to higher temperatures in the reactor, which reduces the rate of conversion. However, it should be noted that since the total number of bubbles is much more for the higher flow rate, the total rate of hydrate formation is higher. Another important factor about Fig. 3e is that the mole fraction flattens out at 13 % since it is very close to maximum theoretical conversion possible for the operating pressure of 3 MPa and equilibrium conditions of the reactor. As the mole fraction of CO₂ decreases in the bubbles, the partial pressure reaches the equilibrium pressure required for hydrate formation and the further conversion is not possible. This challenge is discussed later and can be addressed by increasing the operating pressure.

Fig. 3f depicts an interesting aspect of hydrate formation in bubble column reactors. The conversion factor (CF) defined in equation (8) is a ratio of CO₂ gas consumed in hydrate formation versus the total amount of CO₂ gas flowing in the reactor. At the higher flow rate, the conversion rate is lower due to higher temperatures in the reactor. Fig. 3f shows a conversion efficiency of 78 % and 67 % for the lower and higher flow rates, respectively under the current operating conditions. This clearly highlights the need for enhanced heat dissipation, and the need for an optimal design to maximize CF, noting that the 78 % CF for the lower flow rate is close to the upper limit and most of the conversion is completed in a 3 m length. While operating at higher flow rates will yield larger mass of hydrates, it will require enhanced heat dissipation capabilities or longer reactors. From a process design standpoint, these findings suggest that three similar reactors operating at a certain flow rate will result in much higher rates of hydrate formation than one reactor with 3X flow rate. Therefore, if the techno-economics of adding more reactors is justifiable, the former would be a better design choice.

3.3. Validation of simulations

The results of the simulations of the baseline case, as described in the previous sub-section can be used to validate the model to a limited extent. The presented baseline simulations were conducted to mimic the experiments conducted by Xu et al. [21]. For a flow rate of $Q=27~\text{L/m}^2$ min, Xu et al. [21] reported CO₂ mole fractions in residual gas phase of 13.6 % whereas our simulations predict residual mole fractions of 12.8 %; this constitutes a very reasonable match. The residual mole fractions can be obtained from the conversion factors shown in Fig. 3f. Interestingly, at the higher flow rate of $Q=81~\text{L/m}^2$ min, the conversion

is lower with residual CO2 mole fractions of 18.03 %. Such reduction in conversion at high gas flow rates is in accordance with multiple studies [21,23]. At the lower flow rate Xu et al. [21], reported that the total gas consumption was 411 L. This value, when converted at STP yields an average hydrate formation rate of 0.5 kg/hr, considering that hydrates start forming after equilibrium pressures are reached inside the reactor. From the current simulations, the hydrate formation rate for the lower flow rate is ~ 1 kg/hr, as calculated from R(z) in equation (7). It would then appear that the present simulations will overpredict the experimental results. However, this discrepancy can be attributed to the fact that the experiments by Xu et al. [21] were not conducted at steady state, and the pressures varied from 0 to 3 MPa. Lower pressures reduce the driving force for hydrate formation and yield lower hydrate conversion, compared to our simulations where the pressure is constant at 3 MPa. Another factor, that can contribute to this discrepancy is that the simulations assume a zero induction time for nucleation, which will overpredict the overall formation rate.

4. Impact of various process-related parameters on hydrate formation

The previous section analyzed a baseline case of gas separation, based on CO_2 hydrate formation. In this section, we examine the influence of various process parameters on hydrate formation.

4.1. Influence of enhanced thermal conductivity of hydrate forming media on hydrate formation

Any increase in temperature of the hydrate forming media will reduce the driving force for hydrate formation, thereby reducing the CO_2 hydrate formation. Multiple experimental studies have explored the influence of enhancing the thermal conductivity on hydrate formation. Thermal conductivity can be enhanced through the use of porous metal foams or by dispersing metal nanoparticles [56–58]. Although these techniques have only been explored in traditional stirred batch reactors, we study the influence of enhanced thermal conductivity on hydrate formation in bubble column reactors. Simulations were conducted with the same parameters as in the previous section, but with the thermal conductivity enhanced by 5X and 10X (such enhancements have been reported in literature).

Fig. 4a and b show the axial variation of the conversion factor for the baseline case, and the two cases with enhanced thermal conductivity. It is clearly seen that the conversion improves significantly upon increasing the thermal conductivity by a factor of 5. The benefits of a thermal conductivity enhancement of 10 are marginal compared to an enhancement of 5. As discussed earlier, Fig. 3a and b show a significant temperature rise in the bottom half of the reactor. Therefore, any enhancement in thermal conductivity specially benefits conversion in the lower part of the reactor. Fig. 4a shows that maximum possible conversion occurs much faster with higher thermal conductivities. A similar trend is seen for in Fig. 4b for the high flow rate case. The total hydrate formation rate follows very similar trends as depicted in Fig. 4; however, its absolute value is higher for the higher flow rate case. All these findings clearly highlight the need for thermal conductivity enhancement inside the reactor, with the objective of reducing the reactor size. At the minimum, our simulations suggest the need for thermal conductivity enhancement in the bottom half of the reactor. Another benefit of using metal foams or nanoparticles in the bottom half of the reactor would be the higher nucleation kinetics. Both foams as well as nanoparticles, will provide nucleation sites, which speeds up overall hydrate formation. Metal surfaces can significantly improve the nucleation kinetics as shown in multiple studies [59-61].

4.2. Influence of bubble size on hydrate formation

The size of the bubbles is an important and controllable parameter in

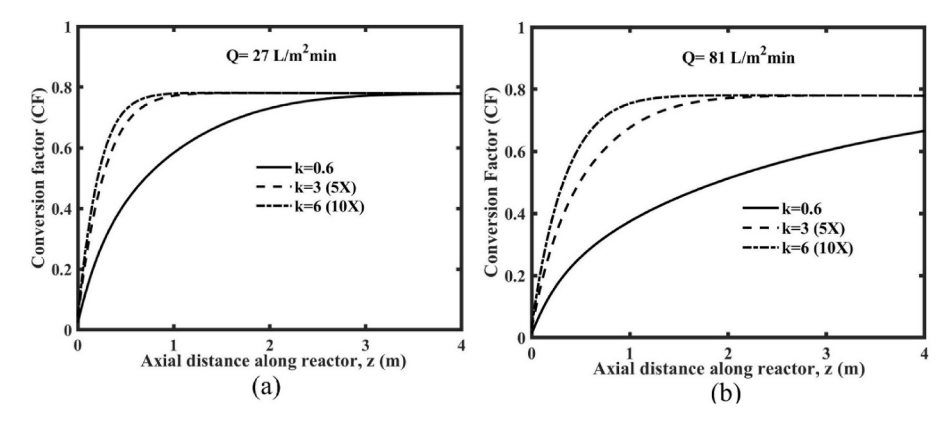


Fig. 4. Influence of thermal conductivity enhancement (of hydrate forming media) for two gas flow rates. The baseline thermal conductivity is 0.6 W/mK.

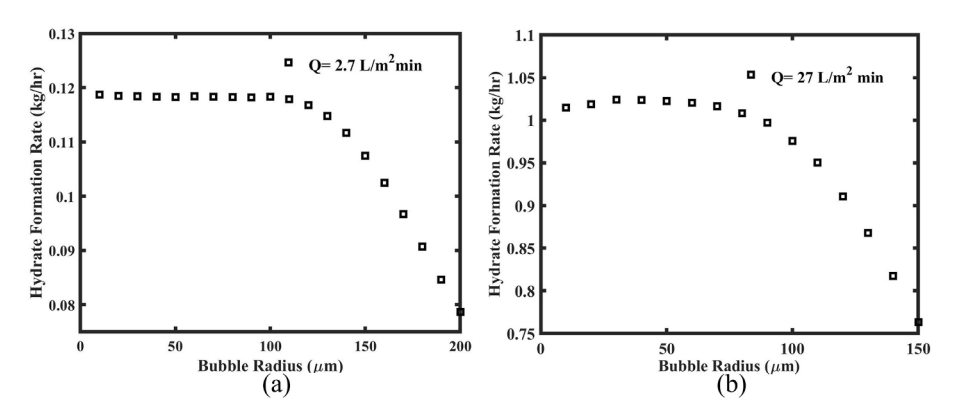


Fig. 5. Influence of bubble size on hydrate formation rate for two gas flow rates.

bubble column reactors. In this section, we simulate the influence of bubble size on the hydrate formation rate, with most other simulation parameters remaining unchanged from the baseline case. The bubble size is varied in the range of 10–200 μm for two gas flow rates, Q=2.7and 27 L/m²min. Smaller bubble size is generally more favorable for hydrate formation due to larger gas-water interfacial contact area. Fig. 5a shows that hydrate formation rate generally increases with decreasing bubble size until it reaches a plateau, thereafter which the increase is not significant. Interestingly, this plateau is reached at a higher bubble size for the lower flow rate case. The maximum hydrate formation rate was achieved for bubbles sizes below 100 μm and 50 μm, for the low and high flow rate cases, respectively. This trend can be attributed to heat accumulation effects in the reactor. Higher heat generation at a higher flow rate slows hydrate formation and will necessitate smaller bubbles to compensate. Overall, these simulations show that operating the reactor at higher flow rates will require smaller bubble sizes to maintain the formation rates.

While smaller bubble sizes aid hydrate formation in general, an interesting result was observed for the larger flow rate case, wherein the hydrate formation rate decreased slightly for very small bubbles. Maximum hydrate formation rate was observed for a bubble size of 30 μm . The decrease in hydrate formation rate for bubbles smaller than 30 μm can be attributed to the excessively high gas—water interfacial area, which generates substantial heat in the bottom part of the reactor (via hydrate formation) and makes overall hydrate formation heat transfer-limited. Xu et al. [21] and Cai et al. [22] reported similar trends in their experiments, where they reported peak hydrate formation rates at a bubble size of $\sim 50~\mu m$. Another detrimental effect of smaller bubble sizes, which is not captured in the simulations is the slow nucleation rate associated with very small bubbles (due to smaller gas—water bubble area for nucleation), which can reduce conversion efficiency. Overall, the present simulations clearly suggest an optimum bubble size to

maximize hydrate formation, with the optimum bubble size decreasing with higher flow rates.

4.3. Influence of reactor pressure on hydrate formation

Hydrate formation occurs in the hydrate stability region at pressures much higher than atmospheric pressure. For hydrate formation from binary gas mixtures, where one gas is non-participating, the hydrate formation pressure depends on the partial pressure of the gas forming the hydrate. For the binary composition of syngas in this study, the

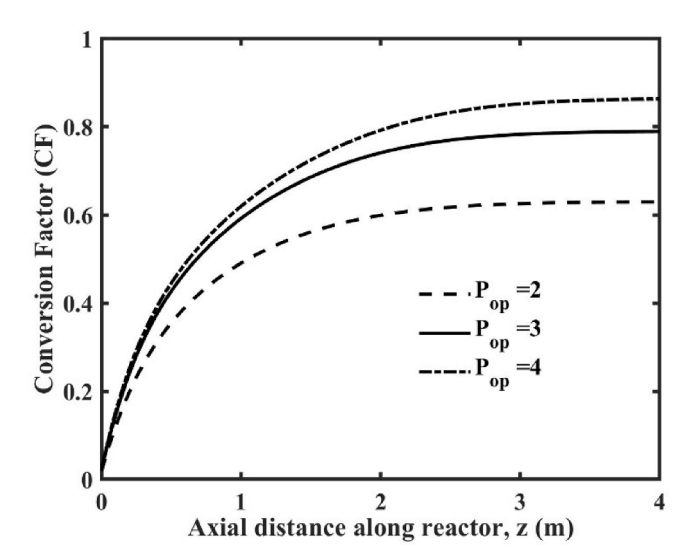


Fig. 6. Influence of reactor pressure on conversion factor.

effective partial pressure exerted by CO_2 decreases with decreasing mole fraction of CO_2 . Hydrate crystallization reduces the mole fraction of CO_2 inside a bubble as it rises in the reactor. Once the CO_2 concentration inside the bubble falls below a certain threshold, the partial pressure of CO_2 is not enough to sustain hydrate formation. This consideration determines the maximum theoretical conversion that can be achieved for specified operating conditions.

The total conversion rate can be improved by increasing the reactor pressure. An increase in reactor pressure will increase the maximum theoretical conversion efficiency by increasing the partial pressures of the gas. Fig. 6 shows the influence of varying the reactor pressure on the total conversion rate. The simulations are conducted for a gas flow rate of 27 L/m²min and depict an increase in conversion of CO₂ into hydrates with increasing pressure. From these simulations, the maximum separation that can be achieved at operating pressures of 2, 3 and 4 MPa are 20.2 %, 12.8 % and 9.6 % mole fraction of residual CO₂ respectively. Such trends were also experimentally observed by Chen et al. [18]. This simulation framework suggests that practical ways to increase the maximum theoretical conversion efficiency include increasing the reactor pressure, or lowering the equilibrium pressures of hydrate formation through the use of thermodynamic promoters. The contribution of hydrostatic pressure and Laplace pressure (due to bubble curvature) to the partial pressure of CO₂ is much smaller than the reactor pressure. Overall, the reactor pressure is an important parameter which determines the maximum separation efficiency in hydrate-based gas separation processes.

4.4. Influence of precooling the inlet gas on hydrate formation

In this sub-section, we analyze the influence of pre-cooling the inlet gas on the steady-state rate of hydrate formation. As discussed previously, one of the key findings of these simulations is the significant rise in temperature in the bottom half of the reactor. Pre-cooling the gas entering the bottom of the reactor can help in minimizing temperature rise, thereby improving the hydrate formation rate. To the best of our knowledge, the influence of a pre-cooled gas on hydrate formation has not been studied before. Fig. 7 shows the influence of precooling the inlet gas to temperatures ranging from 260 to 272 K in reactors with diameters of 11.28 cm and 22.56 cm. The total flow rate is 0.81 L/min and corresponds to the flow rate of 81 L/m²min (flow rate per unit area) in the 11.28 cm diameter reactor, used in the baseline simulations. It is noted that the flow rate is not at STP but rather at the temperature and pressure conditions at the bottom of the reactor. Overall, it is seen that pre-cooling can enhance the hydrate formation rate by upto 5 %.

The plot in Fig. 7 leads to two interesting observations. Firstly, since

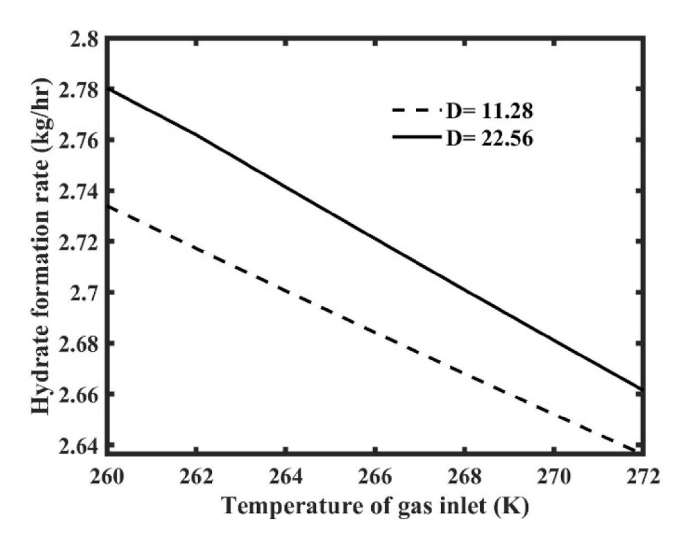


Fig. 7. Influence of pre-cooling the inlet gas on hydrate formation rate.

the total gas flow rate is the same, it is expected that the larger diameter reactor will provide higher hydrate formation rate, since heat generation (due to hydrate crystallization) is spread out over a larger volume, which reduces the volumetric heat generation. Moreover, pre-cooling the underside of the reactor further enhances the hydrate formation rate for the larger diameter reactor. This is due to the larger surface area providing larger cooling effect on the underside of the reactor. Secondly, because of the bigger reactor providing a larger cooling effect, the benefits of pre-cooling become more significant with higher levels of pre-cooling. This is evident from the fact that the slope of line corresponding to D = 22.56 cm is higher than that of 11.28 cm. Therefore, the enhancement in hydrate formation rate at lower pre-cooling (like 260 K) is higher for the bigger reactor. In addition to the above-mentioned benefits, pre-cooling can also significantly increase the nucleation rate of hydrates. Overall, our simulations highlight key advantages of precooling the reactor, especially, for reactors with large cross-sectional area.

4.5. Influence of diameter and height of reactor on hydrate formation

This section analyzes the influence of the diameter and height of the reactor on the rate of hydrate formation. For this analysis, the total gas flow rate is kept the same as that in the previous sub-section (0.81 L/min). All other parameters remain unchanged. It is noted that since the diameter is varied, the gas flow rate per unit area through the bottom of the reactor is not constant. A constant total flow rate ensures that the total gas available for hydrate formation is constant.

Fig. 8 shows the variation in hydrate formation rate with the diameter of the reactor for three heights of the reactor. In general, hydrate formation rate increases with diameter. There are two competing heat transfer effects that increase or decrease the hydrate formation rate inside the reactor. An increase in diameter of the reactor reduces the volumetric heat generation since the total gas flow rate is the same. The reduced volumetric heat generation decreases the temperature rise inside the reactor (upon hydrate formation), thereby increasing hydrate formation rate. However, as the reactor diameter increases, heat dissipation from the center to the outer parts of the reactor is impeded, which will result in a temperature rise, thereby decreasing the hydrate formation rate. Both these effects compete with each other. Our simulations show that for diameters > 1 m, hydrate formation rate does not increase linearly, but rather increases at a much slower rate. For a long reactor (height of 5 m), the hydrate formation rate reaches a maximum at a diameter of 1.5 m. The "heat diffusion impeded regime" is shown in Fig. 8 and indicates the region where the limitations on heat diffusion

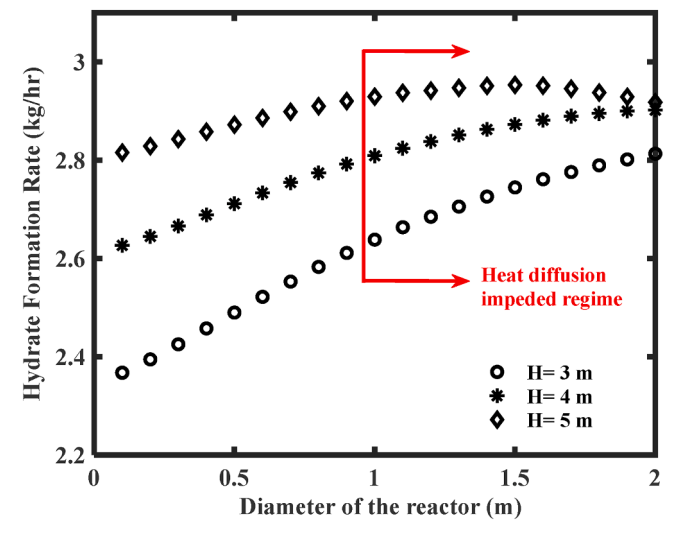


Fig. 8. Influence of diameter of the reactor on hydrate formation rate.

affect hydrate formation rate.

It should be noted that although hydrate formation rate increases for larger sized reactors, the reactor cost and weight increase as well. For a flow rate of 0.81 L/min, simulations show that a 1 m diameter reactor will be adequate from a process efficiency standpoint. Moreover, Fig. 8 also shows that longer reactors increase the hydrate formation rate due to better hydrate conversion achieved over the length of the reactor. However, increasing the height of reactor will also increase the cost and weight. The fact that the presently developed modeling framework can analyze such tradeoffs highlights its utility as a tool to design reactors.

5. Conclusions

This article presents a novel physics-based simulation framework to predict hydrate growth in bubble column reactors; importantly this model accounts for the influence of coupled heat and mass transfer on hydrate formation. Several phenomena dealing with mass transfer, heat transfer and interfacial chemistry are included in the governing equations. This modeling framework is used to quantify the impact of various operating parameters (gas flow rate, bubble size, reactor pressure, inlet gas temperature, reactor diameter) on hydrate formation rate and gasto-hydrate conversion factor. Simulations are benchmarked with limited experimental data available from another study, which used hydrate formation to separate CO_2 from syngas.

These simulations result in several findings and insights related to the complex transport phenomena that govern gas hydrate formation. The results clearly highlight the significant negative impact of inadequate heat removal from the reactor on hydrate formation rate and conversion factor. Enhancing the thermal conductivity of the hydrate forming media can significantly enhance hydrate formation, with an estimated 2X increase in conversion factor. By analyzing various tradeoffs associated with bubbles, it is seen that bubbles smaller than 100 µm diameter are essential to realize high hydrate growth rates. Increasing the reactor pressure can significantly improve the maximum theoretical separation efficiency. Simulations show that maximum theoretical separation efficiency for CO₂ can be > 90 % for moderately high reactor pressures. Precooling the inlet gas is another process parameter that can be used to enhance hydrate formation. Finally, this simulation framework can analyze the influence of reactor size on various phenomena which influence heat generation and dissipation. Overall, the generalized formulation and findings from this work can greatly assist in the design and optimization of bubble column reactors for hydrate formation for syngas separation and other applications.

Declaration of Competing Interest

The authors declare that they have no known competing financial interests or personal relationships that could have appeared to influence the work reported in this paper.

Data availability

Code has been uploaded to Mendeley Data

Acknowledgements

The authors acknowledge National Science Foundation CBET-1653412 for supporting this work. The authors thank Prof. Ofodike Ezekoye from the Walker Department of Mechanical Engineering, UT Austin for his comments on convergence of numerical schemes. The authors thank Dr. Serhat Bilyaz from UT Austin for his help in running the simulation codes on TACC (Texas Advanced Computing Center) resources. The assistance of Awan Bhati from UT Austin in preparing Fig. 2 is also acknowledged.

Appendix A. Supplementary data

Supplementary data to this article can be found online at https://doi.org/10.1016/j.cej.2022.139322.

References

- [1] E.D. Sloan, Coh C.A. Clathrate hydrate of natural gases. 2007. doi: 10.1201/9781420008494.
- [2] Makogon Y. F. Hydrates of Hydrocarbons. 1997. https://www.osti.gov/biblio/ 665385.
- [3] A. Hassanpouryouzband, E. Joonaki, M. Vasheghani Farahani, S. Takeya, C. Ruppel, J. Yang, et al., Gas hydrates in sustainable chemistry, Chem Soc Rev 49 (2020) 5225–5309, https://doi.org/10.1039/c8cs00989a.
- [4] Z. Yin, M. Khurana, H.K. Tan, P. Linga, A review of gas hydrate growth kinetic models, Chem Eng J 342 (2018) 9–29, https://doi.org/10.1016/j.cej.2018.01.120.
- [5] A. Vysniuskas, P.R. Bishnoi, A kinetic study of methane hydrate formation, Chem Eng Sci 38 (1983).
- [6] Englezos P, Kalogerakis N, Dholabhai PD, Bishnoi PR. Kinetics of formation of methane and ethane gas hydrates 1987;42.
- [7] P. Skovborg, P. Rasmussen, A mass transport limited model for the growth of methane and ethane gas hydrates, Chem Eng Sci 49 (1994) 1131–1143, https:// doi.org/10.1016/0009-2509(94)85085-2.
- [8] J.M. Herri, J.S. Pic, F. Gruy, M. Cournil, Methane hydrate crystallization mechanism from in-situ particle sizing, AIChE J 45 (1999) 590–602, https://doi. org/10.1002/aic.690450316.
- [9] X. Fu, L. Cueto-felgueroso, R. Juanes, Nonequilibrium Thermodynamics of Hydrate Growth on a Gas-Liquid Interface, Phys Rev Lett 144501 (2018) 1–6, https://doi. org/10.1103/PhysRevLett. 120.144501.
- [10] H. Liang, D. Guan, K. Shi, L. Yang, L. Zhang, J. Zhao, Characterizing Mass-Transfer mechanism during gas hydrate formation from water droplets, Chem Eng J 428 (2022), 132626. https://doi.org/10.1016/j.cej.2021.132626.
- [11] H. Dashti, D. Thomas, A. Amiri, X. Lou, Variations of the shrinking core model for effective kinetics modeling of the gas hydrate-based CO2 capture process, Computer Aided Chemical Engineering 46 (2019) 1687–1692, https://doi.org/ 10.1016/B978-0-12-818634-3.50282-4.
- [12] D.J. Turner, K.T. Miller, S.E. Dendy, Methane hydrate formation and an inward growing shell model in water-in-oil dispersions, Chem Eng Sci 64 (2009) 3996–4004, https://doi.org/10.1016/j.ces.2009.05.051.
- [13] P. Linga, M.A. Clarke, A review of reactor designs and materials employed for increasing the rate of gas hydrate formation, Energy Fuels 31 (2017) 1–13, https:// doi.org/10.1021/acs.energyfuels.6b02304.
- [14] A. Li, L. Jiang, S. Tang, An experimental study on carbon dioxide hydrate formation using a gas-inducing agitated reactor, Energy 134 (2017) 629–637, https://doi.org/10.1016/j.energy.2017.06.023.
- [15] G. Zhang, X. Shi, F. Wang, Methane hydrate production using a novel spiral-agitated reactor: Promotion of hydrate formation kinetics, AIChE J 68 (2022) 5–7, https://doi.org/10.1002/aic.17423.
- [16] P. Babu, R. Kumar, P. Linga, Pre-combustion capture of carbon dioxide in a fixed bed reactor using the clathrate hydrate process, Energy 50 (2013) 364–373, https://doi.org/10.1016/j.energy.2012.10.046.
- [17] F. Rossi, M. Filipponi, B. Castellani, Investigation on a novel reactor for gas hydrate production, Appl Energy 99 (2012) 167–172, https://doi.org/10.1016/j. apenergy.2012.05.005.
- [18] Z. Chen, J. Fang, C. Xu, Z. Xia, K. Yan, X. Li, Carbon dioxide hydrate separation from Integrated Gasification Combined Cycle (IGCC) syngas by a novel hydrate heat-mass coupling method, Energy 199 (2020), 117420, https://doi.org/ 10.1016/j.energy.2020.117420.
- [19] S. Hashemi, A. Macchi, P. Servio, Gas-liquid mass transfer in a slurry bubble column operated at gas hydrate forming conditions, Chem Eng Sci 64 (2009) 3709–3716, https://doi.org/10.1016/j.ces.2009.05.023.
- [20] Y.T. Luo, J.H. Zhu, S.S. Fan, G.J. Chen, Methane hydrate formation kinetics in bubble column reactors.pdf, Chem Eng Sci 62 (2007) 1000–1009.
- [21] C.G. Xu, L.X. Sen, Q.N. Lv, Z.Y. Chen, J. Cai, Hydrate-based CO2 (carbon dioxide) capture from IGCC (integrated gasification combined cycle) synthesis gas using bubble method with a set of visual equipment, Energy 44 (2012) 358–366, https://doi.org/10.1016/j.energy.2012.06.021.
- [22] J. Cai, C.G. Xu, Z.M. Xia, Z.Y. Chen, L.X. Sen, Hydrate-based methane separation from coal mine methane gas mixture by bubbling using the scale-up equipment, Appl Energy 204 (2017) 1526–1534, https://doi.org/10.1016/j. apenergy.2017.05.010.
- [23] J. Cai, C. Xu, Z. Xia, Z. Chen, X. Li, Hydrate-based Methane Recovery from Coal Mine Methane Gas in Scale-up Equipment with Bubbling, Energy Procedia 105 (2017) 4983–4989, https://doi.org/10.1016/j.egypro.2017.03.996.
- [24] Q.N. Lv, L.X. Sen, C.G. Xu, Z.Y. Chen, Experimental investigation of the formation of cyclopentane-methane hydrate in a novel and large-size bubble column reactor, Ind Eng Chem Res 51 (2012) 5967–5975, https://doi.org/10.1021/ie202422c.
- [25] Y. Xin, J. Zhang, Y. He, C. Wang, Modelling and experimental study of hydrate formation kinetics of natural gas-water-surfactant system in a multi-tube bubble column reactor, Can J Chem Eng 97 (2019) 2765–2776, https://doi.org/10.1002/ cice. 23515
- [26] Xu H, Khan MN, Peters CJ, Sloan ED, Koh CA. Hydrate-Based Desalination Using Cyclopentane Hydrates at Atmospheric Pressure. J Chem Eng Data 2018;63: 1081–7. doi: 10.1021 /acs.jced.7b00815.

- [27] Y. Luo, J. Zhu, G. Chen, Numerical Simulation of Separating Gas Mixtures via Hydrate Formation in Bubble Column, Chinese J Chem Eng 15 (2007) 345–352, https://doi.org/10.1016/s1004-9541(07)60091-3.
- [28] W. Fu, Z. Wang, B. Sun, L. Chen, A mass transfer model for hydrate formation in bubbly flow considering bubble-bubble interactions and bubble-hydrate particle interactions, Int J Heat Mass Transf 127 (2018) 611–621, https://doi.org/ 10.1016/j.ijheatmasstransfer.2018.06.015.
- [29] L.E. Zerpa, E.D. Sloan, A.K. Sum, C.A. Koh, Overview of CSMHyK: A transient hydrate formation model, J Pet Sci Eng 98–99 (2012) 122–129, https://doi.org/ 10.1016/j.petrol.2012.08.017.
- [30] Qin H, Qu A, Wang Y, Zerpa L, Koh C, Bodnar S, et al. Predicting Hydrate Plugging Risk in Oil Dominated Systems using a Transient Hydrate Film Growth Prediction Tool. Offshore Technol. Conf. Houston, Texas, 2020, p. OTC-30545-MS.
- [31] A. Kar, A. Bhati, P.V. Acharya, A. Mhadeshwar, P. Venkataraman, T.A. Barckholtz, et al., Diffusion-based modeling of film growth of hydrates on gas-liquid interfaces, Chem Eng Sci 234 (2021), 116456, https://doi.org/10.1016/j.ces.2021.116456.
- [32] Susilo R, Ripmeester JA, Englezos P. Characterization of gas hydrates with PXRD, DSC, NMR, and Raman spectroscopy. Chem Eng Sci 2007;62:3930–9. doi: 10.1016 /i.ces.2007.03.045.
- [33] Kar A, Acharya P, Bhati A, Shahriari A, Mhahdeshwar A, Barckholtz TA, Bahadur V, Modeling the influence of heat transfer on gas hydrate formation. Summer Heat Transf. Conf. ASME, 2022, p. HT2022-79744.
- [34] L. Mu, S. Li, Q. Ma, K. Zhang, C. Sun, G. Chen, Fluid Phase Equilibria Experimental and modeling investigation of kinetics of methane gas hydrate formation in waterin-oil emulsion, Fluid Phase Equilib 362 (2014) 28–34, https://doi.org/10.1016/j. fluid 2013 08 028
- [35] T.B. Charlton, L.M. Di, L.E. Zerpa, C.A. Koh, M.L. Johns, E.F. May, et al., Simulating Hydrate Growth and Transport Behavior in Gas-Dominant Flow, Energy Fuels 32 (2018) 1012–1023, https://doi.org/10.1021/acs.energyfuels.7b02199.
- [36] Gootam D, Gaikwad N, Kumar R, Kaisare N. Modeling Growth Kinetics of Methane Hydrate in Stirred Tank Batch Reactors. ACS Eng Au 2021;1:148–59. doi: 10.1021/acsengineeringau.1c00012.
- [37] Y. Wang, J.C. Feng, L.X. Sen, Y. Zhang, G. Li, Analytic modeling and large-scale experimental study of mass and heat transfer during hydrate dissociation in sediment with different dissociation methods, Energy 90 (2015) 1931–1948, https://doi.org/10.1016/j.energy.2015.07.029.
- [38] K. Carpenter, V. Bahadur, Electronucleation for Rapid and Controlled Formation of Hydrates, J Phys Chem Lett 7 (2016) 2465–2469, https://doi.org/10.1021/acs. inclust.6001166
- jpclett.6b01166.

 [39] D.N. Glew, M.L. Haggett, Kinetics of formation of ethylene oxide hydrate. Part I.

 Experimental method and congruent solutions. Can J Chem 46 (1968).
- [40] H.P. Veluswamy, A. Kumar, R. Kumar, P. Linga, An innovative approach to enhance methane hydrate formation kinetics with leucine for energy storage application, Appl Energy 188 (2017) 190–199, https://doi.org/10.1016/j. apenergy.2016.12.002.
- [41] A. Kumar, O.S. Kushwaha, P. Rangsunvigit, P. Linga, R. Kumar, Effect of additives on formation and decomposition kinetics of methane clathrate hydrates: Application in energy storage and transportation, Can J Chem Eng 94 (2016) 2160–2167, https://doi.org/10.1002/cjce.22583.
 [42] Li Sheng-Li, Sun Chang-Yu, Liu Bei, Li Zhi-Yun, Chen Guang-Jin, Sum AK. New
- [42] Li Sheng-Li, Sun Chang-Yu, Liu Bei, Li Zhi-Yun, Chen Guang-Jin, Sum AK. New observations and insights into the morphology and growth kinetics of hydrate films. Sci. Rep. 2014; 4:4129.
- [43] Kundu PK, Cohen IM, Dowling DR. Fluid Mechanics, Elsevier Publications, Sixth Edition.

- [44] G.A. Melhem, R. Saini, B.M. Goodwin, A modified Peng-Robinson equation of state, Fluid Phase Equilib. 47 (1989) 189–237, https://doi.org/10.1016/0378-3812(89) 80176-1
- [45] N. Kantarci, F. Borak, K.O. Ulgen, Bubble column reactors, Process Biochem. 40 (2005) 2263–2283, https://doi.org/10.1016/j.procbio.2004.10.004.
- [46] V. Tesar, Microbubble smallness limited by conjunctions, Chem Eng J 231 (2013) 526–536, https://doi.org/10.1016/j.cej.2013.06.051.
- [47] M.K.H. Al-Mashhadani, S.J. Wilkinson, W.B. Zimmerman, Airlift bioreactor for biological applications with microbubble mediated transport processes, Chem Eng Sci 137 (2015) 243–253, https://doi.org/10.1016/j.ces.2015.06.032.
- [48] D. Dapelo, J. Bridgeman, A CFD strategy to retrofit an anaerobic digester to improve mixing performance in wastewater treatment, Water Sci Technol 81 (8) (2020) 1646–1657, https://doi.org/10.2166/wst.2020.086.
- [49] W.B. Zimmerman, M.K.H. Al-Mashhadani, H.K.H. Bandulasena, Evaporation dynamics of microbubbles, Chem Eng Sci 101 (2013) 865–877, https://doi.org/ 10.1016/j.ces.2013.05.026.
- [50] T. Maekawa, Equilibrium Conditions for Carbon Dioxide Hydrates in the Presence of Aqueous Solutions of Alcohols, Glycols, and Glycerol, J. Chem. Eng. Data 1280–4 (2010).
- [51] A.H. Mohammadi, A. Eslamimanesh, V. Belandria, D. Richon, Phase Equilibria of Semiclathrate Hydrates of CO2, N2, CH4, or H2 + Tetra- n -butylammonium Bromide Aqueous Solution, J. Che. Eng. Data (2011) 3855–3865.
- [52] T. Uchida, T. Ebinuma, J. Kawabata, H. Narita, Microscopic observations of formation processes of clathrate-hydrate films at an interface between water and carbon dioxide, J Cryst Growth 204 (1999) 348–356, https://doi.org/10.1016/ S0022-0248(99)00178-5.
- [53] B.Z. Peng, A. Dandekar, C.Y. Sun, H. Luo, Q.L. Ma, W.X. Pang, et al., Hydrate film growth on the surface of a gas bubble suspended in water, J Phys Chem B 111 (2007) 12485–12493, https://doi.org/10.1021/jp074606m.
- [54] M. Akyurt, G. Zaki, B. Habeebullah, Freezing phenomena in ice-water systems, Energy Convers Manag 43 (2002) 1773–1789, https://doi.org/10.1016/S0196-8904(01)00129-7.
- [55] K.G. Libbrecht, Physical Dynamics of Ice Crystal Growth, Annu Rev Mater Res 47 (2017) 271–295, https://doi.org/10.1146/annurev-matsci-070616-124135.
- [56] S. Fan, L. Yang, X. Lang, Y. Wang, D. Xie, Kinetics and thermal analysis of methane hydrate formation in aluminum foam, Chem Eng Sci 82 (2012) 185–193, https://doi.org/10.1016/j.ces.2012.07.040.
- [57] R. Li, D. Liu, L. Yang, G. Cui, J. Wang, X. Wang, et al., Rapid methane hydrate formation in aluminum honeycomb, Fuel 252 (2019) 574–580, https://doi.org/ 10.1016/i.fuel.2019.04.160.
- [58] O. Nashed, B. Partoon, B. Lal, K.M. Sabil, A. Mohd, Review the impact of nanoparticles on the thermodynamics and kinetics of gas hydrate formation, J Nat Gas Sci Eng 55 (2018) 452–465, https://doi.org/10.1016/j.jngse.2018.05.022.
- [59] A. Kar, P.V. Acharya, A. Bhati, A. Mhadeshwar, P. Venkataraman, T.A. Barckholtz, H. Celio, F. Mangolini, V. Bahadur, Magnesium-Promoted Rapid Nucleation of Carbon Dioxide Hydrates, ACS Sustain Chem Eng 9 (2021) 11137–11146, https://doi.org/10.1021/acssuschemeng.1c03041.
- [60] P.V. Acharya, A. Kar, A. Shahriari, A. Bhati, A. Mhadeshwar, V. Bahadur, Aluminum-Based Promotion of Nucleation of Carbon Dioxide Hydrates, J Phys Chem Lett 11 (2020) 1477–1482, https://doi.org/10.1021/acs.jpclett.9b03485.
- [61] A. Kar, A. Bhati, M. Lokanathan, V. Bahadur, Faster Nucleation of Ice at the Three-Phase Contact Line: Influence of Interfacial Chemistry, Langmuir 37 (2021) 12673–12680, https://doi.org/10.1021/acs.langmuir.1c02044.
- $[62] \ \ BCR-hydrate-codes, \ Mendeley \ Data, \ DOI: \ 10.17632/5w38ddrc47.1.$